Atmospheric Research 330 (2026) 108621

Contents lists available at ScienceDirect

Atmospheric Research

journal homepage: www.elsevier.com/locate/atmosres

Distinct climate drivers governing the dominant interannual variability of co-occurrences of heat and ozone pollution extremes over northern and southern urban clusters in Eastern China

Xuejie Zhong [a,b], Pinya Wang [a,b,*], Yang Yang [a,b], Hong Liao [a,b], Jianping Tang [c]

[a] State Key Laboratory of Climate System Prediction and Risk Management/Jiangsu Key Laboratory of Atmospheric Environment Monitoring and Pollution Control/Jiangsu Collaborative Innovation Center of Atmospheric Environment and Equipment Technology/Joint International Research Laboratory of Climate and Environment Change, Nanjing University of Information Science and Technology, Nanjing, Jiangsu, China

[b] School of Environmental Science and Engineering, Nanjing University of Information Science and Technology, Nanjing, Jiangsu, China

[c] School of Atmospheric Sciences, Nanjing University, Nanjing, Jiangsu, China

ARTICLE INFO

Keywords:
Co-occurrences of heat and ozone pollution extremes
Interannual variability
Climate drivers
Teleconnections

ABSTRACT

Under global warming, Eastern China faces severe challenges from co-occurrences of heat and ozone (O_3) pollution extremes (CHOEs). Utilizing long-term observational data, two dominant modes of interannual variability in the summer frequency of CHOEs over Eastern China during 2000–2022 are identified with empirical orthogonal function (EOF) analysis. The leading two modes account for nearly 50 % of the total variance. The first mode (EOF1) exhibits a positive anomaly center over the North China Plain (NCP). EOF1 is associated with increased springtime snow cover in Eastern Europe. The thermal anomalies due to snowmelt trigger Rossby wave trains that propagate eastward along the mid-latitude westerly jet, modulating local circulation and consequently CHOE anomalies over NCP. The second mode (EOF2) features a dipole pattern with intensified positive anomalies over the southern urban clusters while weaker negative anomalies in the north. For EOF2, a La Niña-like sea surface temperature pattern induces Rossby waves that propagate along the subtropical jet stream. Meanwhile, springtime sea ice loss over the Barents Sea trigger southeastward propagating wave trains. The combined effects of these remote drivers modulate the local atmospheric circulation across southern urban clusters, ultimately regulating the anomalous CHOE frequency. These findings not only deepen our understanding of the large-scale climate drivers shaping the dominant modes of CHOEs over Eastern China, but also highlight the distinctive teleconnection pathways between northern and southern urban clusters, offering a scientific basis for improving early warning and regional mitigation strategies.

1. Introduction

Under global warming, extreme heat events have become increasingly intense, frequent, and long-lasting across the globe (Martinez-Villalobos et al., 2025; Liu et al., 2024; Yuan et al., 2025), imposing profound impacts on socio-economic systems, ecosystems, and public health (He et al., 2022; Zou et al., 2025; Luthi et al., 2023; Gong et al., 2025). Particularly, Eastern China, covering the central and eastern parts of the country and characterized by dense population, has experienced a significant intensifying trend of summer heatwaves in recent decades (Ji and Chen, 2024; Kong et al., 2020). For instance, the record-breaking heatwave in summer of 2022 swept most of Eastern China, accompanied by prolonged drought conditions, and many sites saw the highest temperature records for more than 60 years during the event (Ma et al., 2023).

On the other hand, Eastern China has experienced severe ozone (O_3) pollution in the past decades. As a typical secondary pollutant, tropospheric O_3 primarily forms through photochemical reactions between volatile organic compounds (VOCs) and nitrogen oxides (NOx) (Chen et al., 2024a; Jiang et al., 2025; Elshorbany et al., 2024). Observational evidence indicate a significant upward trend in surface O_3 concentrations across China (Lu et al., 2020; Weng et al., 2022; Zhang et al.,

* Corresponding author at: State Key Laboratory of Climate System Prediction and Risk Management/Jiangsu Key Laboratory of Atmospheric Environment Monitoring and Pollution Control/Jiangsu Collaborative Innovation Center of Atmospheric Environment and Equipment Technology/Joint International Research Laboratory of Climate and Environment Change, Nanjing University of Information Science and Technology, Nanjing, Jiangsu, China.
E-mail address: pinya.wang@nuist.edu.cn (P. Wang).

https://doi.org/10.1016/j.atmosres.2025.108621
Received 2 September 2025; Received in revised form 22 October 2025; Accepted 4 November 2025
Available online 5 November 2025

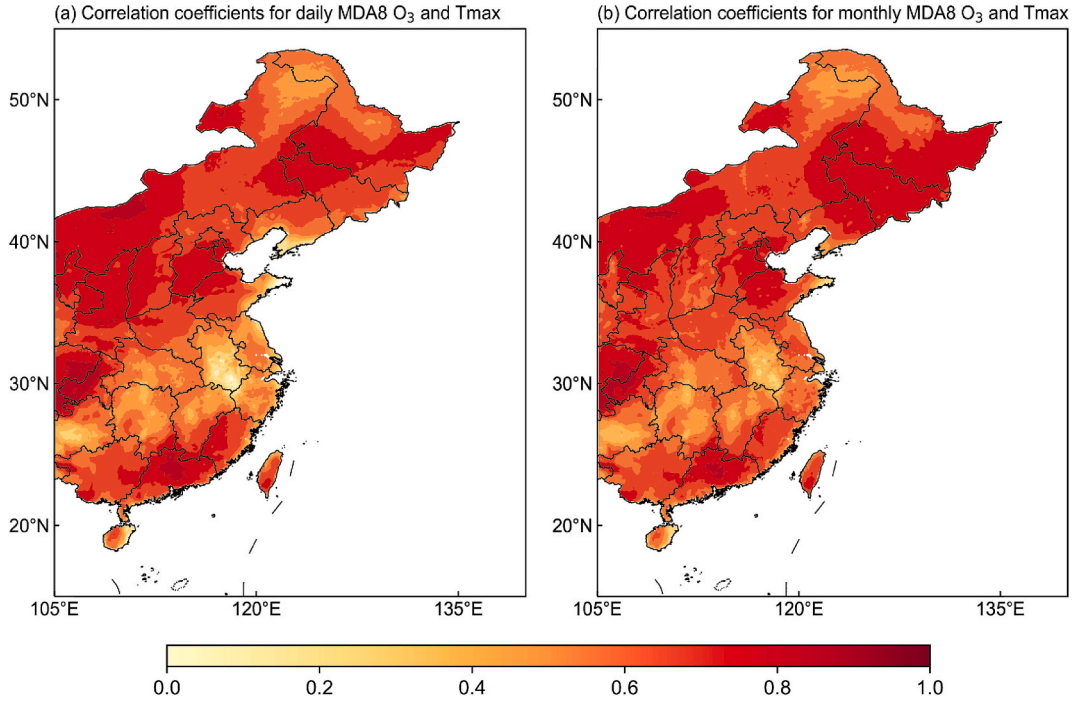

Fig. 1. Spatial distributions of the correlation coefficients between Tmax and MDA8 O_3 in summer during 2000–2022 over Eastern China. (a) Correlation based on daily Tmax and daily MDA8 O_3. (b) Correlation based on monthly mean Tmax and monthly mean MDA8 O_3.

2020), posing substantial threats to public health and ecosystems (Li et al., 2022a; Liu et al., 2018; Zheng et al., 2018). The megacity clusters such as the North China Plain (NCP), Yangtze River Delta (YRD), and Pearl River Delta (PRD) have become O_3 pollution hotspots due to intensive anthropogenic emissions (Li et al., 2019; Lu et al., 2018; Yin et al., 2019). While precursor emissions establish the baseline for O_3 production, meteorological factors play a critical role in modulating its spatiotemporal variability through photochemical and transport processes (Yang et al., 2024; Gong and Liao, 2019; Kou et al., 2023). In particular, extreme heat events are conducive to O_3 pollution, primarily through two pathways. First, elevated temperatures directly accelerate the photochemical reaction rates of O_3 precursors, thereby promoting O_3 formation (Lee et al., 2014; Kong et al., 2025; Coates et al., 2016). Second, extreme heat events are often accompanied by specific meteorological conditions favorable for O_3 accumulation, such as persistent high-pressure systems, low wind speeds, and intense solar radiation, which collectively foster atmospheric stagnation (Kerr et al., 2020; Li et al., 2020). These factors suppress the vertical mixing and horizontal dispersion of air pollutants, leading to elevated O_3 concentrations. Therefore, projected more frequent and intense extreme heat events may promote O_3 pollution in the future (Wang et al., 2022; Chen et al., 2024b).

In fact, the compound extreme events characterized by co-occurrences of heat and ozone pollution extremes (CHOEs) have become increasingly prevalent in Eastern China (Li et al., 2024; Wang et al., 2022). The economically developed and densely populated megacity clusters such as the NCP, YRD, and Chengdu-Chongqing urban agglomeration have become hotspots for these compound hazards (Wang et al., 2022; Xiao et al., 2022). The Coupled Model Intercomparison Project Phase 6 (CMIP6) multi-model projections under the high-emission scenario (SSP5–8.5) indicate that growing energy demand and rising greenhouse gas concentrations may further exacerbate the spatiotemporal expansion of the CHOE events (Ban et al., 2022; Gong et al., 2022; Li et al., 2024). Notably, the compound extremes exhibit nonlinear amplification of health impacts that the mortality rates caused by CHOEs significantly exceed those from individual stressors (Krug et al., 2019), this highlights the urgent need to investigate mechanistic drivers of such compound events.

Current works on CHOEs primarily focus on the effects of local synoptic weather conditions (Wang et al., 2022; Wang et al., 2023; Yang et al., 2025a). However, the potential of snow cover, sea surface temperature (SST), and sea ice have received less attention, despite their potential effects on mid-latitudes and even tropical climates through large-scale teleconnections mediated by land-atmosphere coupling, ocean-atmosphere interactions and planetary scale wave dynamics (Deng et al., 2020; Li et al., 2016; Sun et al., 2021; Wu et al., 2010). Wei et al. (2023) pointed out that the decadal intensification of heatwaves over China in recent decades are associated with the concurrent phase transitions of different climate modes, El Niño–Southern Oscillation (ENSO), Atlantic Multidecadal Oscillation (AMO), and Indian Ocean Dipole (IOD), highlighting the role of climate modes in regulating regional extreme events. Therefore, elucidating these processes is essential for advancing the compound risk assessment and developing proactive mitigation strategies.

Therefore, this study focuses on summer CHOEs during 2000–2022 in Eastern China (east of 105°E; see Fig. 1), which is particularly vulnerable to CHOEs (Gao et al., 2023; Wang et al., 2022). We aim to identify their dominant modes and investigate the associated local and remote climatic drivers. The remainder of the paper is structured as follows: Section 2 describes the data and methodology; Section 3 analyzes the spatial distribution and interannual variations of CHOEs; Section 4 examines their dominant modes of CHOE frequency; Section 5 explores the driving factors and associated mechanisms underlying the dominant modes of CHOEs; Section 6 provides the summary and discussion.

2. Data and Methods

2.1. Observed ozone concentrations

Surface MDA8 O_3 concentrations ($\mu g/m^3$) for 2000–2022 were obtained from the ChinaHighO_3 dataset-a high-resolution (0.1° × 0.1°), quality-assured product for China (Wei et al., 2022; Yang et al., 2025b). This dataset demonstrates robust performance, with out-of-sample/out-

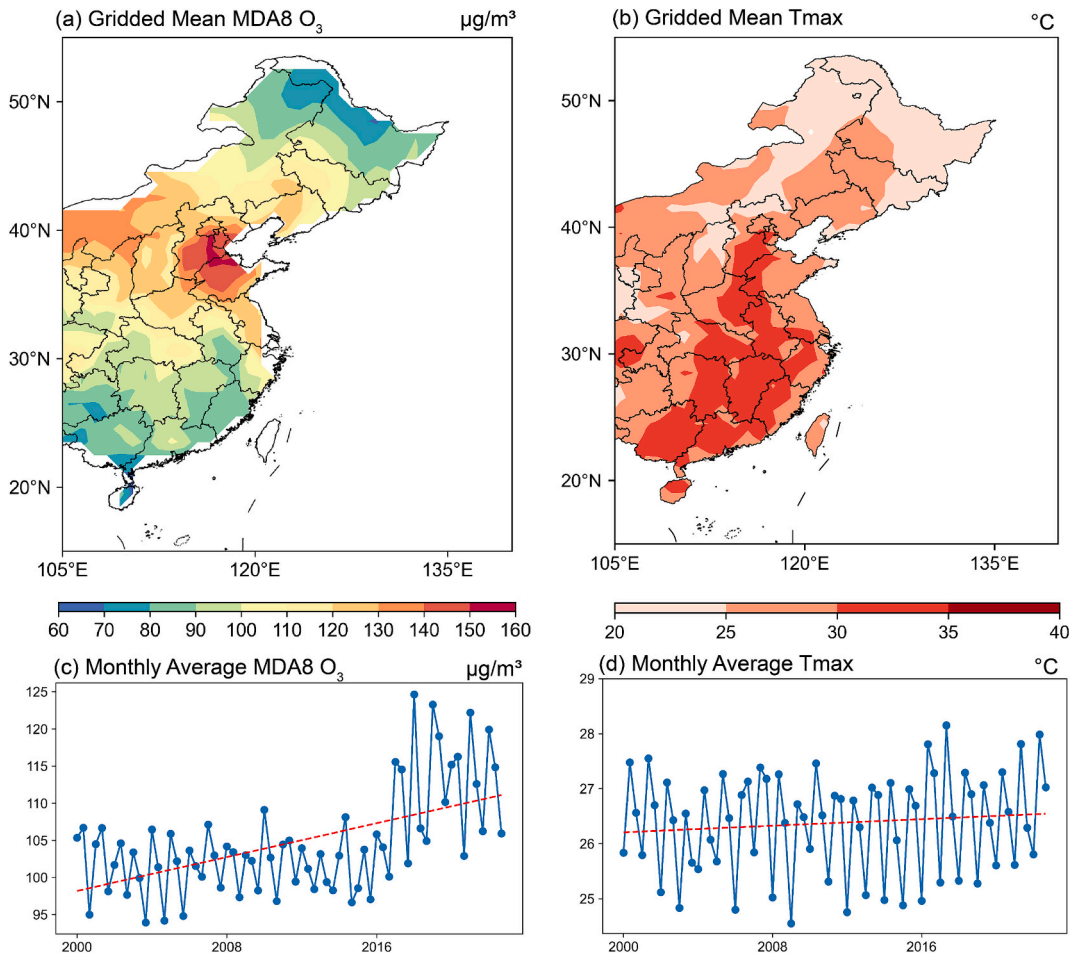

Fig. 2. Spatial distributions of (a) gridded mean MDA8 O_3, and (b) gridded mean Tmax during summer for 2000–2022 in Eastern China. (c) Time series of the monthly average MDA8 O_3 and (d) Tmax in summer. Blue line indicate monthly mean values, and red trend lines reflect long-term linear trends. (For interpretation of the references to colour in this figure legend, the reader is referred to the web version of this article.)

of-station validation yielding mean coefficient of determination of 0.87 (0.80) and a root mean square error of 17.10/21.10 μg/m^3 nationally (Wei et al., 2022). Its reliability has established ChinaHighO_3 as a benchmark resource for O_3 pollution studies (Qi et al., 2024; Xu et al., 2024b).

2.2. Reanalysis data

Meteorological parameters including 2 m air temperature (T2m), relative humidity (RH), surface solar radiation downward (SSRD), geopotential height (HGT), eastward wind (uwnd), northward wind (vwnd), sea level pressure (SLP), total cloud cover (TCC) are obtained from the latest fifth generation of the European Centre for Medium-Range Weather Forecasts (ECMWF) reanalysis data (ERA5), which is the latest global atmospheric reanalysis of ECMWF (Hersbach et al., 2020). Monthly snow water equivalent (SWE) from the land component of the ERA5 dataset (ERA5-Land). Monthly mean SST data and monthly mean sea ice concentration (SIC) data are provided by the Hadley Centre Sea Ice and SST dataset version 1, with a spatial resolution of $1^\circ \times 1^\circ$.

2.3. Identification of co-occurrences of heat and ozone pollution extremes (CHOEs)

An O_3 pollution day is identified according to the ambient air quality standards (GB 30952012), with maximum daily 8-h average (MDA8) O_3 concentration exceeded 160 μg/m^3 (Gong and Liao, 2019; Lu et al., 2018; Zong et al., 2022). Extreme heat days are defined as days with daily maximum T2m (Tmax) exceeding 35 °C, consistent with China Meteorological Administration standards (Li and Huang, 2011; Pu et al., 2017). The CHOE days are identified when extreme heat and O_3 pollution days occur concurrently. It's been proved that the selected absolute thresholds effectively capture the upper tail of historical extremes of air temperature and surface O_3 concentrations (not shown) while maintaining direct relevance to significant health and environmental risks.

2.4. Wave activity flux

The wave activity flux (WAF) is a useful diagnostic tool for illustrating a "snapshot" of a propagating packet of stationary wave trains. In this study, we adopt the Takaya-Nakamura (T-N) wave activity flux (Takaya and Nakamura, 2001) to investigate the dynamical processes underlying the teleconnections associated with the dominant modes of CHOEs. The T-N flux is particularly suitable for diagnosing wave propagation on a zonally varying background flow and can effectively depict both the direction and magnitude of stationary Rossby wave energy propagation. The horizontal component of WAF is estimated by (Takaya and Nakamura, 2001):

$$W = \frac{p}{2a^2|V|}\left\{\begin{array}{l} \dfrac{\overline{u}}{\cos\varphi}\left[\left(\dfrac{\partial\psi'}{\partial\lambda}\right)^2 - \psi'\dfrac{\partial^2\psi'}{\partial\lambda^2}\right] + \overline{v}\left[\dfrac{\partial\psi'}{\partial\lambda}\dfrac{\partial\psi'}{\partial\varphi} - \psi'\dfrac{\partial^2\psi'}{\partial\lambda\partial\varphi}\right] \\ \overline{u}\left[\dfrac{\partial\psi'}{\partial\lambda}\dfrac{\partial\psi'}{\partial\varphi} - \psi'\dfrac{\partial^2\psi'}{\partial\lambda\partial\varphi}\right] + \overline{v}\cos\varphi\left[\left(\dfrac{\partial\psi'}{\partial\varphi}\right)^2 - \psi'\dfrac{\partial^2\psi'}{\partial\varphi^2}\right] \end{array}\right\} \quad (1)$$

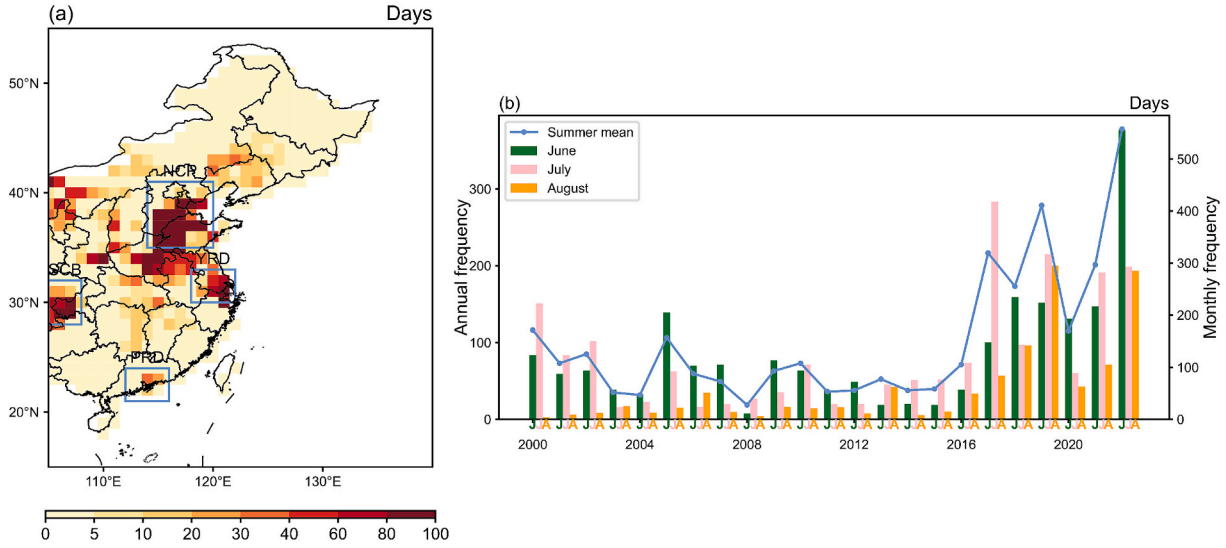

Fig. 3. Spatial distribution and temporal variations of CHOE frequency (days). (a) Spatial distribution of CHOE frequency for all summers during 2000–2022. (b) Interannual variations of CHOE frequency during summer (per month), aggregated over all grid cells within the Eastern China domain (blue line), along with monthly counts (colored bars). The four major urban clusters are outlined by blue boxes, including the North China Plain (NCP; 32–40°N, 114–121°E), Yangtze River Delta (YRD; 30–33°N, 118–122°E), Pearl River Delta (PRD; 21–24°N, 112–116°E), and Sichuan Basin (SCB; 28–32°N, 105–108°E). (For interpretation of the references to colour in this figure legend, the reader is referred to the web version of this article.)

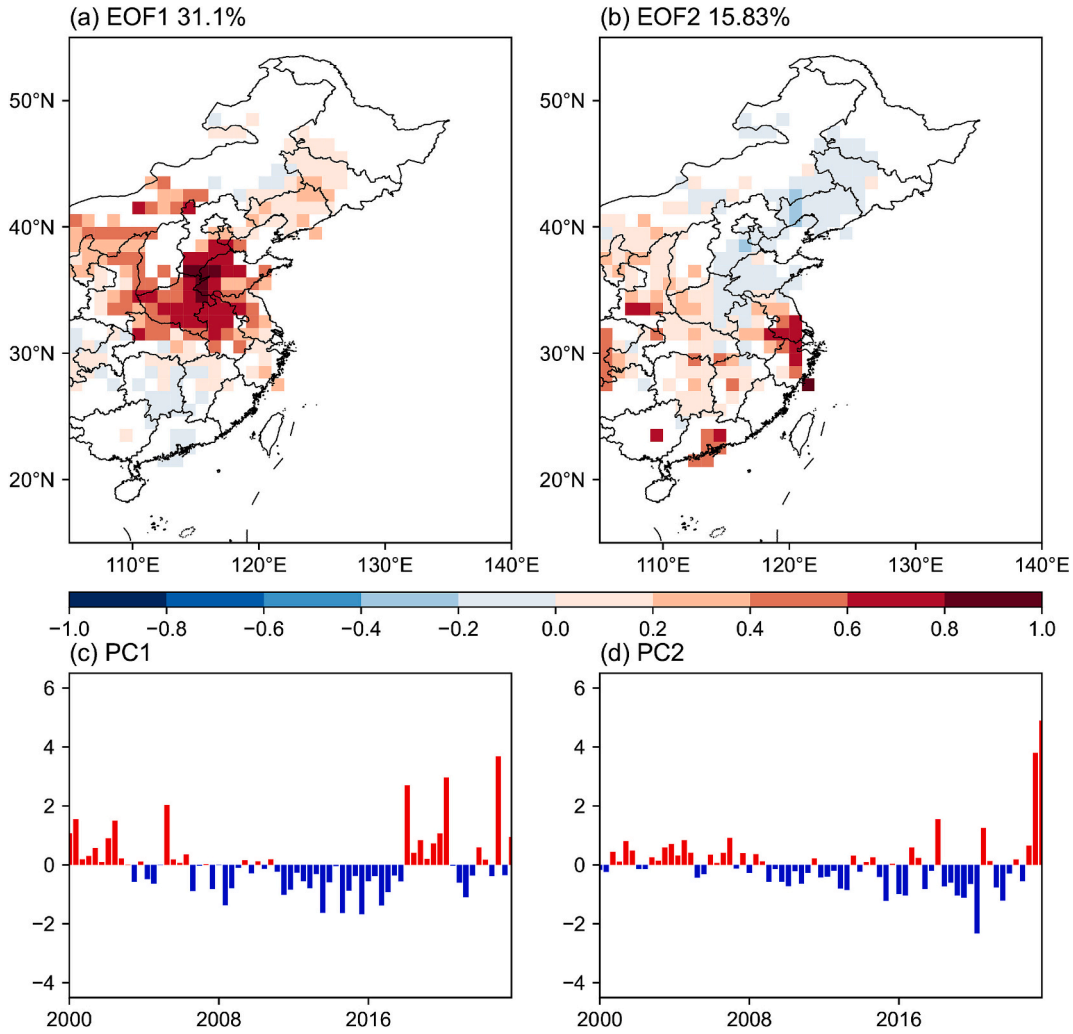

Fig. 4. Leading modes of summer CHOEs frequency derived from EOF analysis during 2000–2022. (a–b) Spatial patterns of the first (EOF1, 31.1 %) and second (EOF2, 15.83 %) modes; (c–d) corresponding principal component (PC) time series showing interannual variations.

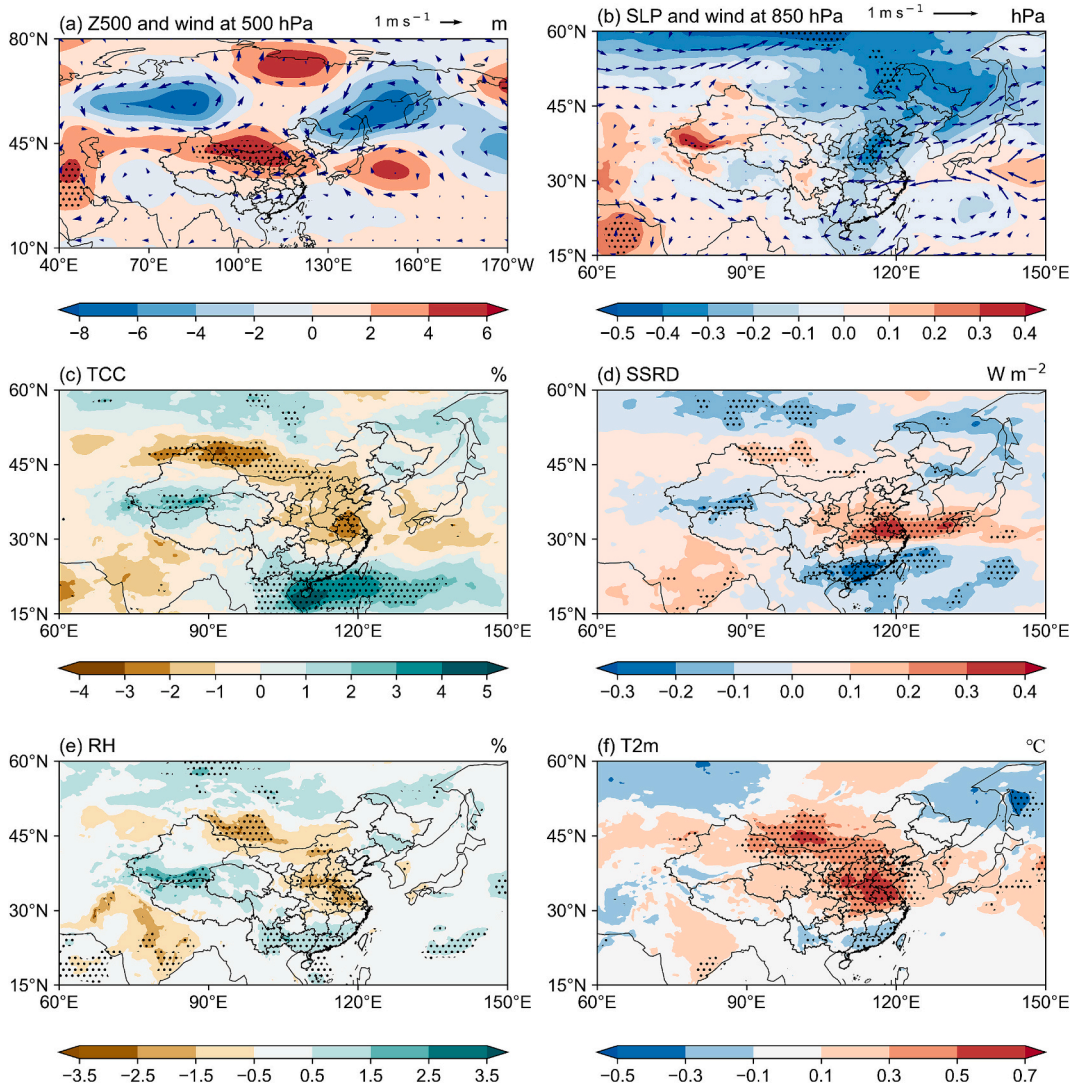

Fig. 5. Meteorological anomalies regressed onto standardized PC1 for: (a) geopotential height (HGT) and winds at 500 hPa, (b) surface level pressure (SLP) and winds at 850 hPa, (c) total cloud cover (TCC), (d) surface solar radiation downward (SSRD), (e) relative humidity (RH), and (f) 2 m air temperature (T2m). Stippling indicate regions with statistically significant anomalies at the 95 % confidence level.

Where p is pressure, and a indicates Earth's radius; λ and φ are longitude and latitude, respectively, with $\overline{u}$ and $\overline{v}$ indicating the horizontal wind components in the corresponding directions; ψ'represents the stream function.

3. Spatiotemporal distributions of CHOEs during 2000–2022

Fig. 1 shows the spatial distribution of the correlation between daily (Fig. 1a) and monthly (Fig. 1b) Tmax and MDA8 O_3 during summer over 2000–2022. High positive correlations are observed across most parts of Eastern China, with coefficients exceeding 0.6 at the daily scale and reaching above 0.7 at the monthly scale across many areas. Particularly strong correlations are found in NCP, YRD, PRD, and Sichuan Basin (SCB) city clusters. These city clusters also exhibit high summer mean levels of both surface O_3 and air temperature (Figs. 2a&b), suggesting a strong co-variability between heat and O_3 pollution on both daily and monthly timescales.

The spatial distribution of the frequency of CHOEs further reflects this co-variability (Fig. 3a). CHOEs occur most frequently in the NCP, SCB, and YRD, where more than 80 days are recorded over the study period. These hotspot regions overlap with areas exhibiting both high correlations and elevated levels of Tmax and MDA8 O_3. The annual variations of CHOE days (Fig. 3b) reveals large interannual variability, with a pronounced increase after 2013. This upward trend corresponds with the long-term increase in both surface O_3 and temperature (Figs. 2c–d), indicating an escalating risk of compound extremes under concurrent climate warming and photochemical pollution enhancement in Eastern China.

4. The dominant modes of CHOE days and the local meteorological conditions

To identify the dominant spatiotemporal variability of CHOEs, an empirical orthogonal function (EOF) analysis was performed on monthly CHOE day during summer months (June–August) for the period 2000–2022 (Fig. 4). Specifically, the monthly CHOE days were linearly detrended for each summer month (June–August) to eliminate long-term trends. Moreover, the 2000–2022 multi-year mean for each corresponding month was subtracted to remove the seasonal cycle.

We focus on the first two leading EOF modes, which account for nearly 50 % of the total variance, with EOF1 and EOF2 explaining 31.1 % and 15.83 %, respectively. EOF1 exhibits a spatially coherent monopole pattern centered over NCP, indicating a regionwide enhancement of CHOE days (Fig. 4a). The corresponding principal

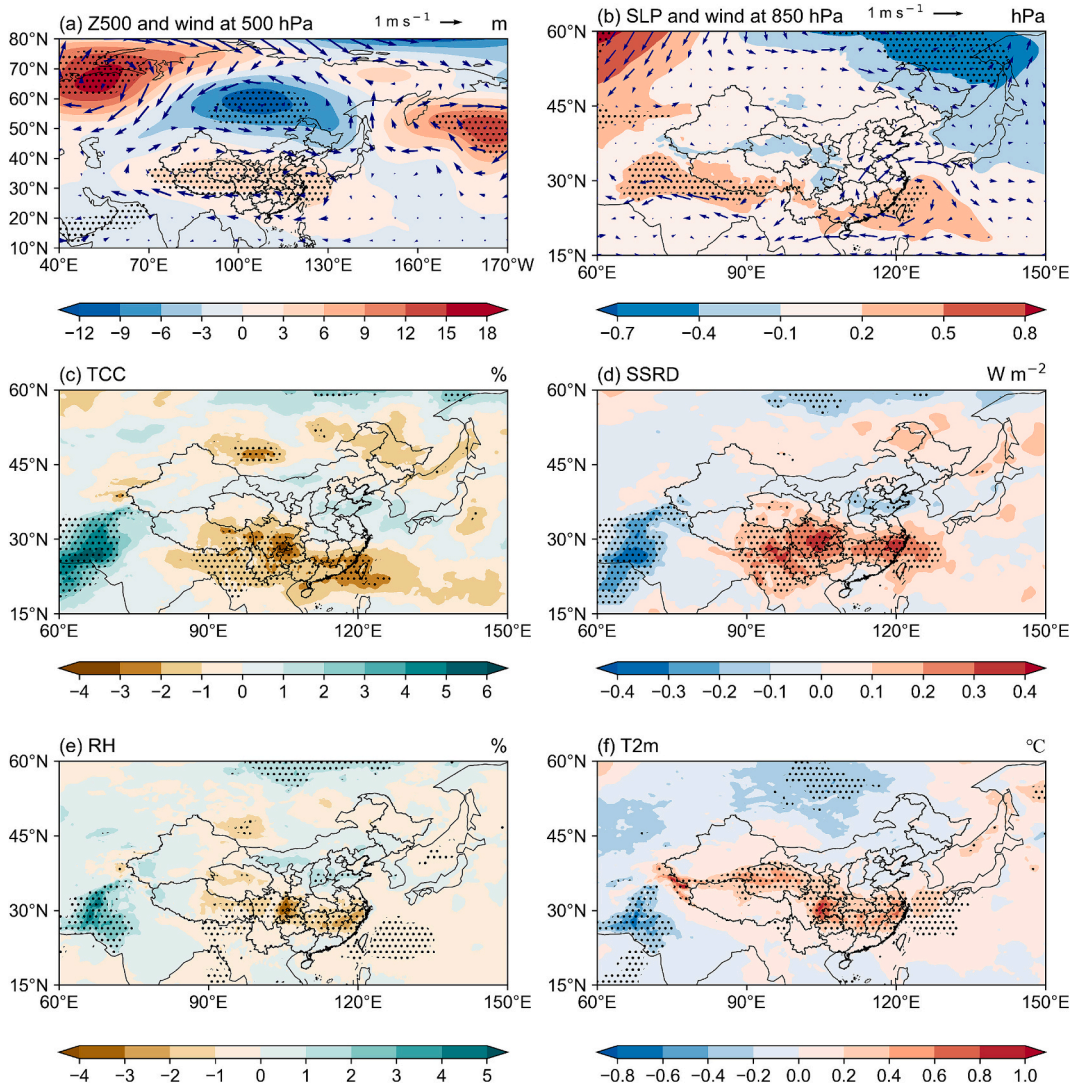

Fig. 6. Same as Fig. 5, but for meteorological anomalies regressed onto standardized PC2.

component (PC1) shows enhanced positive-phase anomalies in recent decade, particularly after 2013, suggesting the intensification of CHOEs under favorable meteorological and chemical conditions (Fig. 4c). In contrast, EOF2 exhibits a north–south dipole pattern, characterized by intensified positive anomalies over the southern urban clusters, indicating a regionally coherent variability in CHOEs across southern China (Fig. 4b). The PC2 time series exhibits pronounced interannual variability, with amplified signals observed since 2016, suggesting an intensification of the EOF2 pattern in recent years (Fig. 4d). In the following, we further explore the meteorological anomalies associated with each EOF mode to uncover the underlying mechanisms that shape the dominant modes of CHOE variability.

For EOF1, which reflects a spatially uniform enhancement in CHOE days centered over the North China Plain, at 500 hPa, a significant anomalous high-pressure system dominates northern China, accompanied by suppressed westerlies and enhanced anticyclonic circulation (Fig. 5a). Near the surface, the anomalous low-level wind fields at 850 hPa exhibit weakened southerlies over Eastern China, indicating reduced ventilation (Fig. 5b), accompanied by negative surface pressure anomalies. Correspondingly, anomalously low total cloud cover (Fig. 5c) and enhanced surface shortwave radiation (Fig. 5d) suggest stronger solar heating, which in turn promotes elevated surface air temperature (Fig. 5f) and suppressed relative humidity (Fig. 5e). These meteorological conditions collectively facilitate O_3 formation (Ma et al., 2021; Tong et al., 2017) and the co-occurrence of heat extremes (Wang et al., 2022), supporting the widespread CHOE pattern captured by EOF1.

For EOF2, at 500 hPa, a negative anomaly occurs in the north and a pronounced positive anomaly is observed over the southern part of Eastern China (Fig. 6a), supporting the meridional dipole pattern of the CHOE frequency anomalies of EOF2. Superimposed on the geopotential height anomalies, the wind field shows an anomalous cyclonic circulation in northern China and an anticyclonic pattern in the south. This is accompanied by positive SLP and low-level anomalous anticyclonic over the south part of China (Fig. 6b), indicating strengthened the western Pacific subtropical high (WPSH) dominating the southern China. Consequently, total cloud cover is significantly reduced (Fig. 6c), and surface shortwave radiation is anomalously enhanced (Fig. 6d). These radiative changes lead to near-surface warming (Fig. 6f) and drying (Fig. 6e), further intensifying the photochemical formation of O_3 (Wang et al., 2024). In contrast, northern China experiences relatively weak circulation anomalies and lacks the pronounced radiative anomalies seen in the south, suggesting a weaker modulation of CHOE events. Overall, EOF2 highlights the dominant role of subtropical high and anticyclonic anomalies over southern China in shaping the local meteorological conditions that favor the CHOE events.

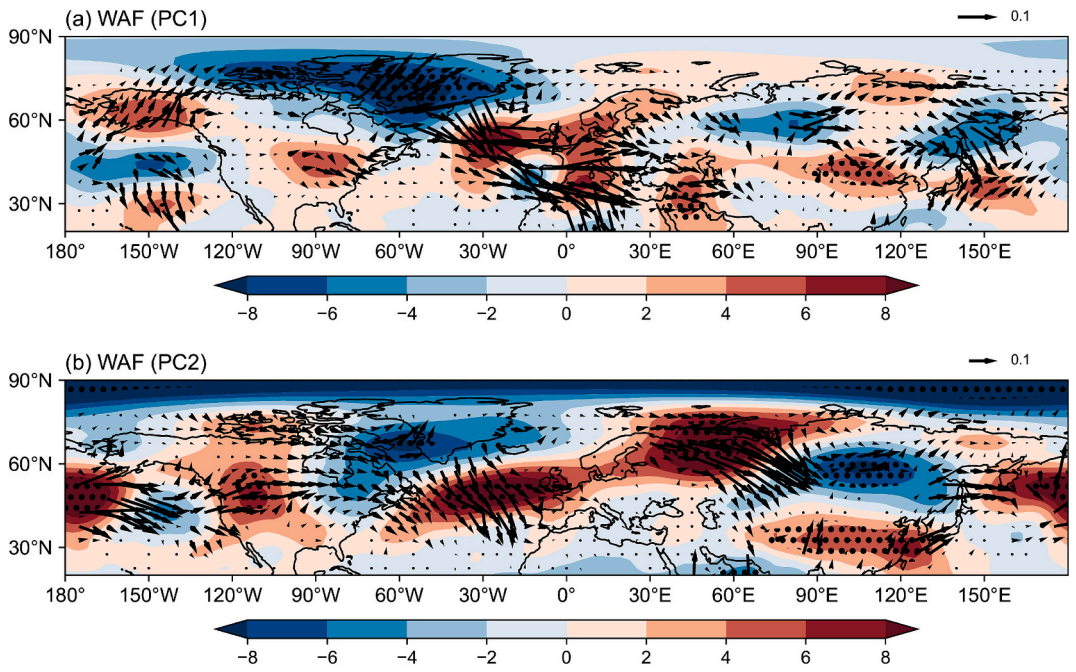

Fig. 7. Regression maps of the 500 hPa wave activity flux ($m^2\ s^{-2}$) and stream function ($m^2\ s^{-1}$) anomalies onto standardized (a) PC1 and (b) PC2. Stippling indicate regions with statistically significant anomalies at the 95 % confidence level.

5. Key drivers and mechanisms of the dominant modes of CHOEs

5.1. Associated wave activity anomalies

The local atmospheric circulation anomalies over China can be modulated by remote driving signals from tropical or high-latitudes through large-scale teleconnections (Li et al., 2022b; Liu et al., 2023; Yin et al., 2018). To further elucidate the potential teleconnection mechanisms underlying the dominant modes of CHOEs, we try to identify signal sources based on the analysis of WAF.

Fig. 7 demonstrates WAF and stream function anomalies at 500 hPa associated with the two leading modes. As shown in Fig. 7a, the WAF vectors associated with EOF1 indicate a well-defined planetary wave train originating from western part of North America, propagating eastward along the midlatitude westerly jet, connected with "negative-positive-negative" stream function anomalies centered over Greenland, North Atlantic and western Europe, and North Eurasia. This wave train induces positive stream function anomalies over North China, corresponds well with the high-pressure anomalies associated with EOF1, thereby triggering or enhancing CHOEs over northern China.

In contrast, the circulation anomalies associated with PC2 exhibit a more complex structure, involving both high-latitude and subtropical wave sources (Fig. 7b). A pronounced wave train emanates from the Barents-Kara Sea region and extends southeastward along the "Arctic-Siberia-southern China" pathway, forming a tripole structure of the stream function anomalies characterized by a "positive-negative-positive" pattern. This high-latitude wave activity highlights the role of Arctic variability in shaping CHOE occurrences over southern China. Simultaneously, another wave train linked to PC2 emerges from the tropical Eastern Pacific and travels eastward along the subtropical jet stream, pointing to the influence of tropical source on East Asian climate through subtropical-extratropical teleconnections. The constructive interference between Arctic originated and tropically forced pathways contributes to the anomalous circulation pattern associated with EOF2.

Notably, the patterns of anomalous wave activities associated with the leading modes are evident at 200 hPa (Fig. S1). Thus, these findings confirm that the two leading CHOE modes are modulated by distinct upstream processes. Specifically, CHOE variability over NCP is primarily controlled by extratropical midlatitude wave dynamics, while CHOE variability over southern urban clusters is driven by the combined

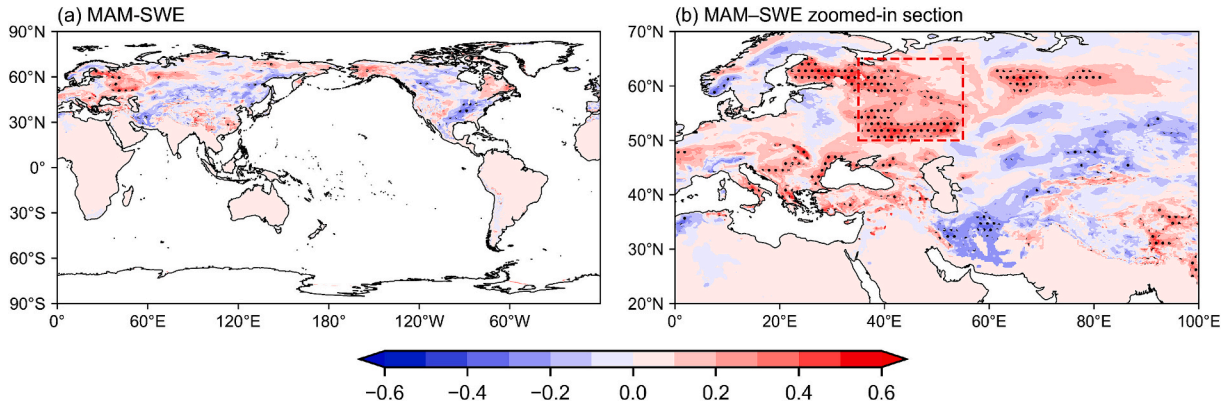

Fig. 8. (a) Spatial correlation pattern between the standardized PC1 and monthly anomalies of spring (MAM) snow water equivalent (SWE). (b) Same as (a), but focusing on the key Eurasian region (20°N–70°N, 0°E–100°E). Stippling indicates regions where correlations are statistically significant at the 95 % confidence level.

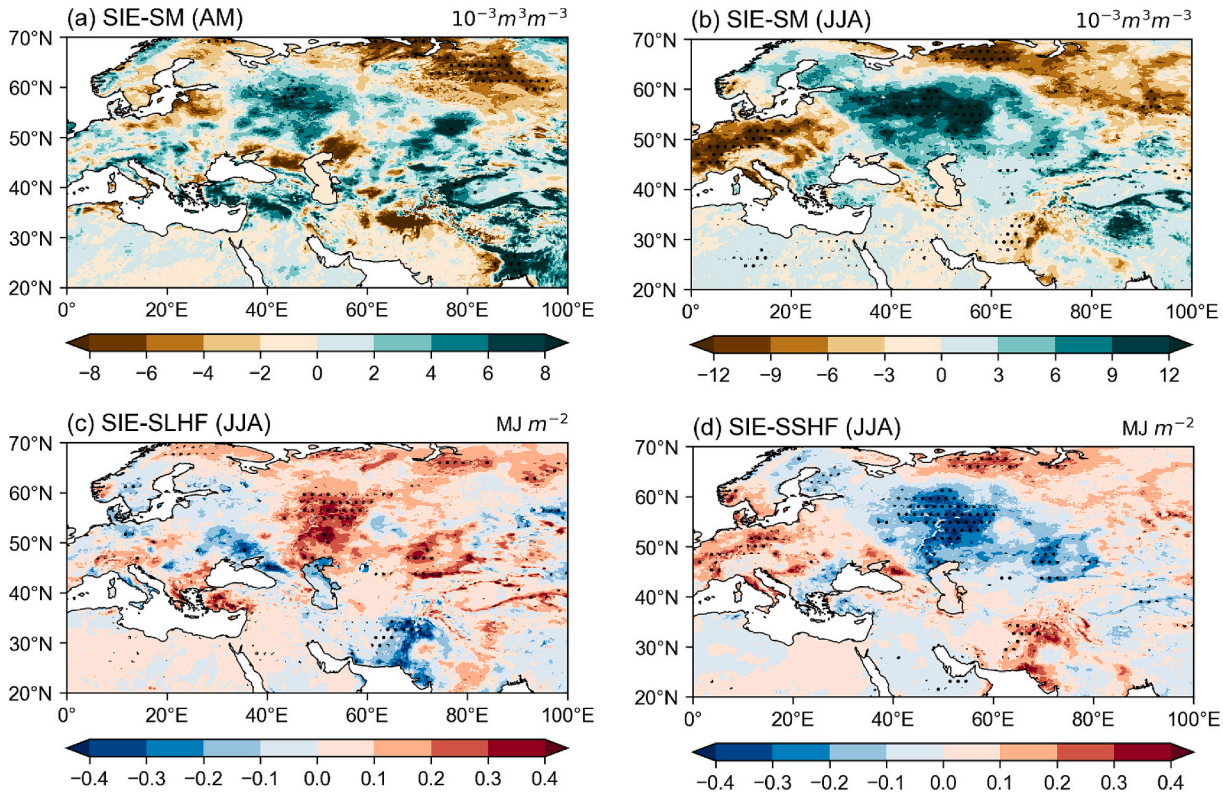

Fig. 9. Regression pattern for 0-7 cm soil moisture (SM) during (a) late spring (April and May), (b) summer (June, July and August), and for (c) surface latent heat flux (SLHF) and (d) surface sensible heat flux during summer onto SIE. Stippling indicates regions where correlations are statistically significant at the 95 % confidence level.

effects of Arctic forcing and tropical forcing.

5.2. *Impacts of spring snow cover on CHOE variability over NCP*

Previous studies have demonstrated a close relationship between springtime snow cover anomalies over the Eurasian continent and the subsequent summer climate over East Asia (Sun et al., 2021; Zhang et al., 2017; Zhou et al., 2021), suggesting that Eurasian springtime snow cover may serve as an important driver of CHOEs. Fig. 8 shows the correlation patterns between snow cover anomalies in the preceding spring and PC1. It can be observed that the springtime snow cover exhibits a significant positive correlation with PC1, which means that increased spring Eurasian snow cover favors increased CHOEs over NCP. Previous studies suggested that this lagged effect may mainly result from the spring snowmelt induced soil moisture (SM) anomalies, which can persist for several weeks to months, and then alter the land surface energy budget and the atmospheric thermal condition in the following season (Sun et al., 2021; Zhang et al., 2025b). To examine if this works for the relationship between spring Eurasia snow cover and SM response, we calculate the area-averaged ERA5-Land SWE over the domain 50°N–65°N, 35°E–55°E as the spring snow cover variability index (SIE). Further analysis reveals that SIE is significantly positively linked to late spring (April–May) SM (Fig. 9a) while SM show insignificant anomalies in March (not shown). This suggests that excessive spring snow cover leads to increased SM during the snowmelt season in late spring, which further persists into summer (Fig. 9b). The increase in SM regulates the land surface energy balance and influences surface–atmosphere heat exchange, manifested by enhanced latent heat flux (Fig. 9c) and reduced sensible heat flux (Fig. 9d), thus affecting the local surface diabatic heating to the atmosphere above.

It is claimed that the persistent thermal anomalies in SM and surface sensible heat induce local geopotential height anomalies and strengthen the eastward-propagating wave train which may cause circulation perturbation over China (Sun et al., 2021), thereby affecting CHOEs over NCP. We further reveal that during years with excessive snow cover in the key region, the local meteorological conditions over NCP in summer exhibit strong resemblance to the circulation anomalies associated with EOF1 discussed earlier (Fig. 5). In particular, a significant positive geopotential height anomaly at 500 hPa is observed over NCP (Fig. 10a), indicating the presence of a warm high-pressure ridge in the mid-to-upper troposphere and enhanced static stability. Meanwhile, SLP shows a positive anomaly over the same region (Fig. 10b), accompanied by divergent winds at 850 hPa, which favors enhanced subsidence. The resulting adiabatic warming associated with the downward motion effectively promotes surface temperature increases (Fig. 10f), further confirming that excessive springtime snow cover can modulate atmospheric circulation and local thermodynamic processes, eventually contributing to the formation of a hot and dry background over NCP in summer that is conducive to the development of CHOEs. These findings further support the notion that springtime snow cover anomalies may serve as an early indicator for CHOEs, highlighting the critical role of land surface processes in linking seasonal snow anomalies to regional extreme climate events.

5.3. *Influence of pre-seasonal sea surface temperature and Arctic Sea ice on CHOEs variability over southern urban clusters*

Fig. 11 demonstrates the regression patterns of SST anomalies from preceding winter to summer onto the normalized PC2. It's noted that the occurrence of CHOEs over the southern part of Eastern China in summer is closely associated with La Niña-like SST anomalies, which is established in the previous winter and persisting into summer. Specifically, the SST anomalies exhibit a characteristic "*Z*-shaped" spatial structure, characterized by significantly cooling SSTs over the equatorial eastern Pacific and positive SST anomalies over the mid to high latitudes of North Pacific. This spatial pattern alters the tropical air-sea thermal

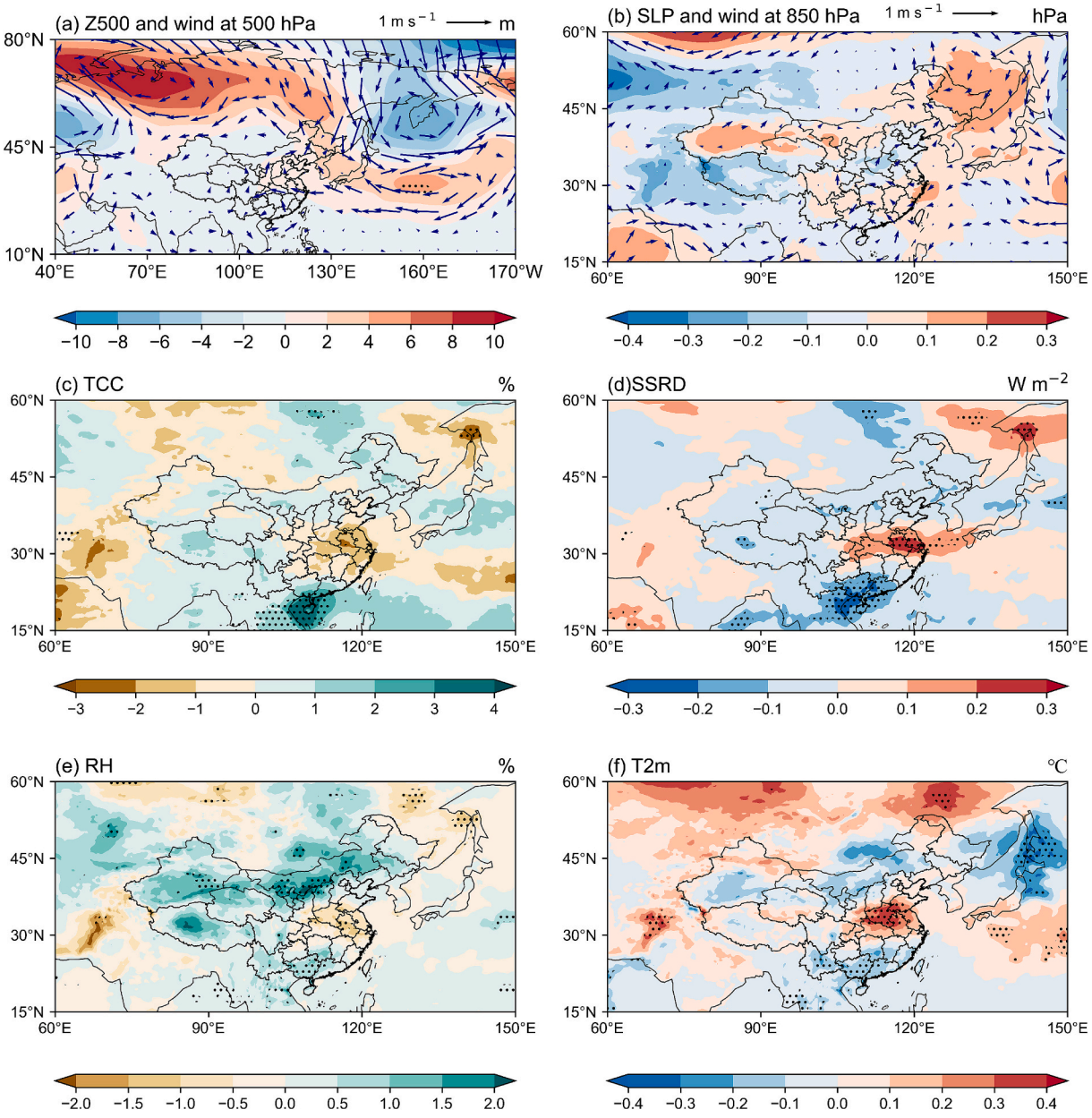

Fig. 10. Regression of local meteorological anomalies on the standardized spring snow cover variability index (SIE): (a) geopotential height (HGT) and winds at 500 hPa, (b) surface level pressure (SLP) and winds at 850 hPa, (c) total cloud cover (TCC), (d)surface solar radiation downward (SSRD), (e) relative humidity (RH), and (f) 2 m air temperature (T2m) anomalies regressed onto standardized SIE. Stippling indicate regions with statistically significant anomalies at the 95 % confidence level.

exchange, substantially enhancing convective activity over the tropical Pacific and increasing its meridional asymmetry (Wen and Li, 2023). Through modifications in the vertical motion associated with the Walker circulation and adjustments in zonal mass transport, these changes excite a large-scale Rossby wave train response (Wu et al., 2010). These disturbances propagate energy and momentum from the tropics to the mid and high latitudes via planetary-scale energy dispersion mechanisms, inducing large-scale circulation anomalies over the North Pacific and Eurasia (as seen in Fig. 7). It could be summarized that the La Niña-like SST anomalies exert a significant remote influence on the local atmospheric circulation patterns over the southern part of Eastern China during summer, thereby modulating the likelihood of CHOEs. This highlights the critical role of ocean-atmosphere interactions in shaping regional extreme climate events.

To further verify the impacts of such anomalous SST pattern over tropical Pacific on EOF2, we select a key region to construct SST index (SSTI), defined as the springtime mean SST averaged over the region 5°N–5°S, 150°W–90°W. The region captures the core of SST anomalies in the central and eastern equatorial Pacific. Springtime SSTI is selected as SST anomalies exhibit the strongest signal. It's demonstrated that a decrease in the SSTI associated anomalously cold SSTs in the central and eastern tropical Pacific suppress convection, resulting in upper tropospheric convergence (Huang et al., 2024; Li et al., 2025). This suppressed convection acts as a negative heating source and exerts Rossby wave trains that propagate northeastward along the subtropical jet stream (Li et al., 2025), and modulate the atmospheric circulation over mid latitudes of Eurasia, as seen in Fig. 7b. Specifically, an anomalous anticyclonic circulation emerges at 500 hPa (Fig. 13a), accompanied by a significant positive sea level pressure anomaly at 850 hPa (Fig. S2a). This enhanced high-pressure system suppresses convective activity,

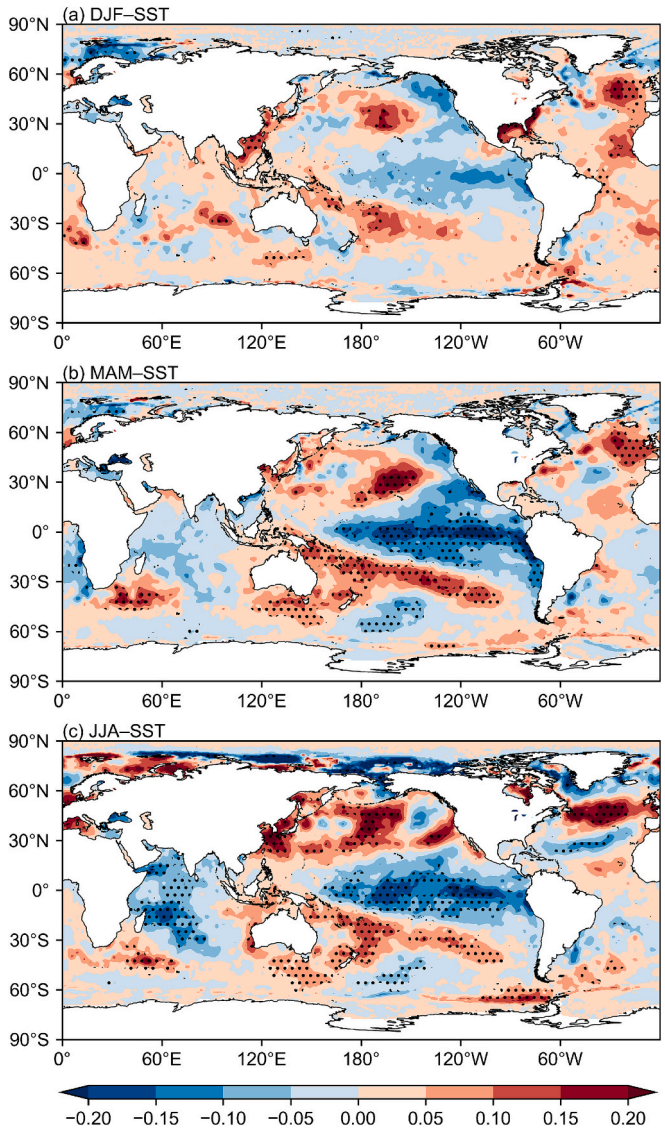

Fig. 11. Regression pattern of SST during (a) DJF, (b) MAM, and (c) JJA onto the standardized PC2. Stippling indicate regions with statistically significant anomalies at the 95 % confidence level.

leading to increased surface shortwave radiation (Fig. S2c) and a marked reduction in relative humidity (Fig. S2d). Consequently, near surface temperatures exhibit a widespread rise, particularly over the southern part of Eastern China (Fig. 13b). In addition, the total cloud cover shows a notable decrease under the influence of the anomalous high pressure (Fig. S2b), further reinforcing the enhancement of solar radiation reaching the surface.

We further focus on the linkage between Arctic Sea ice loss and the CHOEs over southern parts of China, as suggested by the wave train propagation in Fig. 7b. Fig. 12 demonstrates the regression pattern of spring sea ice concentration (SIC) associated with EOF2. A pronounced decline in spring SIC over the Barents Sea is significantly related to the increasing frequency of CHOEs in the southern part of Eastern China (Fig. 12a), and the reduction gradually weakens into summer months (Fig. 12b). The significant reduction in SIC in the Barents Sea contributes to the Arctic amplification through the synergistic effects of sea ice-albedo and sea ice-cloud feedback mechanisms (Goosse et al., 2018). Moreover, these SIC anomalies trigger the Rossby wave train propagating eastward towards East Asia (Fig. 7b), ultimately influencing the atmospheric circulation structure over East Asia. To further elucidate the effects of SIC loss over Barents Sea on CHOEs in Eastern China, we define Barents Sea Ice Concentration index (SICBS), the average SIC over the core region (30°E–55°E, 77.5°N–82.5°N; Fig. 12a). We find that reduced SICBS is associated with anomalous downward motion over the southern part of Eastern China (Fig. 13c), increased net shortwave radiation (Fig. S3c), and positive temperature anomalies (Fig. 13d), favoring the increasing CHOEs over southern urban city clusters of China.

6. Discussion and conclusions

As two closely linked global challenges, climate warming and air pollution have contributed to the increasing frequency of CHOEs over Eastern China, with dense population and concentrated industrial activities. CHOEs represent a complex atmospheric-environmental issue arising from the interplay of meteorological conditions and physicochemical processes. In this work, we investigate the leading two modes of CHOE frequencies in Eastern China from 2000 to 2022, elucidate the corresponding anomalous atmospheric circulation patterns, and investigate their underlying connections with key climatic factors.

EOF1 is centered over NCP, while EOF2 is characterized by multi-city clusters encompassing the SCB, YRD, and PRD. Together, these two modes account for nearly half of the total explained variance, underscoring their dominant role in shaping CHOEs variability across Eastern China. Further analysis demonstrates that EOF1 is positively correlated with springtime Eurasian snow cover, where snowmelt variations modulate soil moisture, acting as a bridge to summer atmospheric circulation anomalies. Such linkage induces subsidence over NCP,

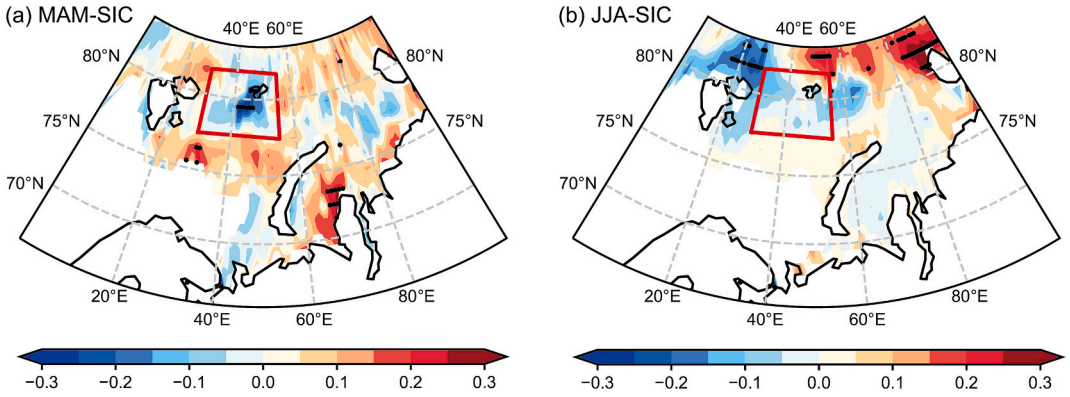

Fig. 12. Regression pattern of Sea ice concentration during (a) MAM and (b) JJA onto normalized PC2. The key region (30°E–55°E, 77.5°N–82.5°N) is outlined with red box. Stippling indicate regions with statistically significant anomalies at the 95 % confidence level. (For interpretation of the references to colour in this figure legend, the reader is referred to the web version of this article.)

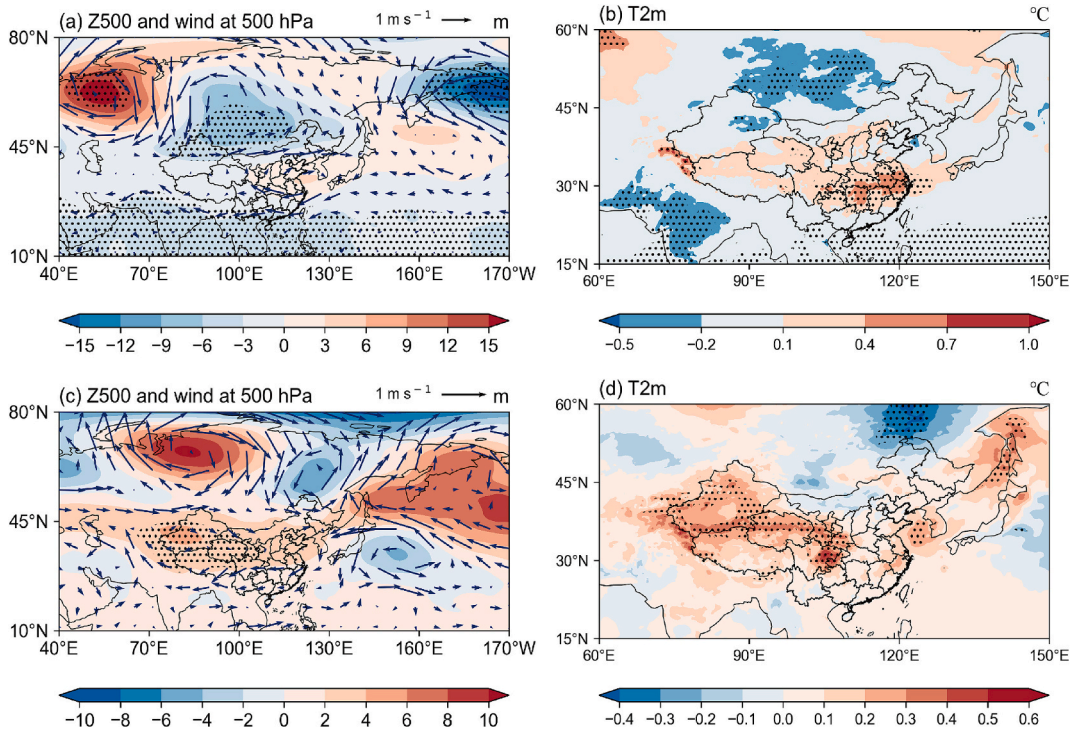

Fig. 13. Regression pattern of geopotential height (HGT) and winds at 500 hPa, and 2 m air temperature (T2m) anomalies onto standardized SSTI (a&b) and SICBS (c&d). Note that SSTI and SICBS are multiplied by −1. Stippling indicate regions with statistically significant anomalies at the 95 % confidence level.

creating favorable conditions for CHOEs occurrence. For EOF2, significant negative correlations are identified with both springtime *Z*-shaped La Niña-like SST anomalies in the tropics and Barents Sea ice extent in the Arctic. These dual forcings alter regional thermal conditions, influence the local atmospheric circulation governing the southern part of Eastern China through exerting the propagation of Rossby wave trains. Apart from these observed relationships, ENSO also plays an important role in modulating regional climate, large-scale atmospheric circulation, and interannual variations of air quality over East Asia (Tang et al., 2025; Zhang et al., 2025a). During El Niño years, the prevailing hot, dry, and cloudless conditions across China favor persistent stagnant weather, which enhances photochemical ozone formation (Jiang and Li, 2022; Li et al., 2022; Yang et al., 2022). In contrast, La Niña episodes often strengthen easterly flow and increase ventilation, thus mitigating surface ozone accumulation (Jeong et al., 2023; Li et al., 2022). Moreover, ENSO can influence stratosphere–troposphere exchange processes. During La Niña phases, stratospheric intrusion events occur more frequently, potentially transporting ozone-rich air into the middle and lower troposphere, further enhancing tropospheric ozone concentrations over East Asia (Wie et al., 2021). These findings suggest that ENSO-driven circulation anomalies likely account for a portion of the observed interannual variability of CHOEs.

Though we primarily focus on the impacts of large-scale climate forcings on spatiotemporal variability of CHOE frequency through comprehensive statistical analyses, limitations should be acknowledged. First, the coupling between anthropogenic emissions and meteorological conditions as well as the roles of physicochemical processes associated with CHOEs warrants further and deeper investigation. It's been demonstrated that the anomalous meteorological conditions during El Niño years, favor persistent stagnant weather across China, which enhances photochemical ozone formation (e.g., Yang et al., 2022). Thus, future studies should prioritize elucidating the multifactorial drivers of CHOEs, particularly under climate change scenarios, with an emphasis on synergistic strategies for anthropogenic emission control and climate change mitigation. In addition, future research should incorporate numerical modeling experiments, such as general circulation models (GCMs) or the linear baroclinic model (LBM), to validate the physical mechanisms proposed in this study, especially the atmospheric circulation responses to specific SST, snow cover, or sea ice anomalies (Xu et al., 2024a; Jia et al., 2025; Chen et al., 2025). Particularly, integrating process-based simulations will be crucial for disentangling the relative contributions of external forcings and internal variability to CHOEs under a changing climate, thereby complementing the statistical insights provided here.

CRediT authorship contribution statement

Xuejie Zhong: Writing – original draft, Visualization, Methodology, Data curation. **Pinya Wang:** Writing – review & editing, Supervision, Methodology, Conceptualization. **Yang Yang:** Supervision, Conceptualization. **Hong Liao:** Supervision. **Jianping Tang:** Supervision.

Declaration of competing interest

The authors declare that they have no known competing financial interests or personal relationships that could have appeared to influence the work reported in this paper.

Acknowledgement

This study was supported by the National Natural Science Foundation of China (Grant 42475032 and 42293323), and the Natural Science Foundation of Jiangsu Province (Grant BK20241902).

Appendix A. Supplementary data

Supplementary data to this article can be found online at https://doi.org/10.1016/j.atmosres.2025.108621.

Data availability

The ground level ozone concentrations are obtained from the high-

resolution and high-quality ground level daily maximum 8 h average ozone (MDA8 O_3) data for the China (ChinaHighO_3) dataset and is open-access and freely available at https://doi.org/10.5281/zenodo.13342827. The ERA5 reanalysis is available at https://doi.org/10.24381/cds.bd0915c6. The monthly mean sea surface temperature and sea ice concentration data can be downloaded via https://www.metoffice.gov.uk/hadobs/hadisst/data/download.html.

References

Ban, J., Lu, K., Wang, Q., Li, T., 2022. Climate change will amplify the inequitable exposure to compound heatwave and ozone pollution. One Earth 5, 677–686. https://doi.org/10.1016/j.oneear.2022.05.007.

Chen, G., Ji, X., Chen, J., Xu, L., Hu, B., Lin, Z., Fan, X., Li, M., Hong, Y., Chen, J., 2024a. Photochemical pollution during summertime in a coastal city of Southeast China: ozone formation and influencing factors. Atmos. Res. 301. https://doi.org/10.1016/j.atmosres.2024.107270.

Chen, T., Wang, T., Xue, L., Brasseur, G., 2024b. Heatwave exacerbates air pollution in China through intertwined climate-energy-environment interactions. Sci. Bull. 69, 2765–2775. https://doi.org/10.1016/j.scib.2024.05.018.

Chen, Y., Wang, H., Zhang, J., Chen, H., Chen, L., Li, D., 2025. Adjustment of Springtime thermal Anomaly Modes over the Tibetan Plateau Altered its Interdecadal Relationship with East Asian Summer Monsoon during the early 2000s. J. Clim. 38, 5857–5877. https://doi.org/10.1175/jcli-d-24-0402.1.

Coates, J., Mar, K.A., Ojha, N., Butler, T.M., 2016. The influence of temperature on ozone production under varying NO_x conditions – a modelling study. Atmos. Chem. Phys. 16, 11601–11615. https://doi.org/10.5194/acp-16-11601-2016.

Deng, K., Jiang, X., Hu, C., Chen, D., 2020. More frequent summer heat waves in southwestern China linked to the recent declining of Arctic Sea ice. Environ. Res. Lett. 15. https://doi.org/10.1088/1748-9326/ab8335.

Elshorbany, Y., Ziemke, J.R., Strode, S., Petetin, H., Miyazaki, K., De Smedt, I., Pickering, K., Seguel, R.J., Worden, H., Emmerichs, T., Taraborrelli, D., Cazorla, M., Fadnavis, S., Buchholz, R.R., Gaubert, B., Rojas, N.Y., Nogueira, T., Salameh, T., Huang, M., 2024. Tropospheric ozone precursors: global and regional distributions, trends, and variability. Atmos. Chem. Phys. 24, 12225–12257. https://doi.org/10.5194/acp-24-12225-2024.

Gao, M., Wang, F., Ding, Y., Wu, Z., Xu, Y., Lu, X., Wang, Z., Carmichael, G.R., McElroy, M.B., 2023. Large-scale climate patterns offer preseasonal hints on the co-occurrence of heat wave and O_3 pollution in China. Proc. Natl. Acad. Sci. 120, e2218274120. https://doi.org/10.1073/pnas.2218274120.

Gong, C., Liao, H., 2019. A typical weather pattern for ozone pollution events in North China. Atmos. Chem. Phys. 19, 13725–13740. https://doi.org/10.5194/acp-19-13725-2019.

Gong, C., Wang, Y., Liao, H., Wang, P., Jin, J., Han, Z., 2022. Future Co-Occurrences of Hot Days and Ozone-Polluted Days over China under scenarios of Shared Socioeconomic Pathways Predicted through a Machine-Learning Approach. Earth's Future 10. https://doi.org/10.1029/2022ef002671.

Gong, J., Shi, X., Wang, C., Zhang, X., 2025. Extreme high temperatures and adaptation by social dynamics: Theory and evidence from China. J. Econ. Behav. Organ. 234. https://doi.org/10.1016/j.jebo.2025.106989.

Goosse, H., Kay, J.E., Armour, K.C., Bodas-Salcedo, A., Chepfer, H., Docquier, D., Jonko, A., Kushner, P.J., Lecomte, O., Massonnet, F., Park, H.S., Pithan, F., Svensson, G., Vancoppenolle, M., 2018. Quantifying climate feedbacks in polar regions. Nat. Commun. 9, 1919. https://doi.org/10.1038/s41467-018-04173-0.

He, B.-J., Wang, J., Zhu, J., Qi, J., 2022. Beating the urban heat: Situation, background, impacts and the way forward in China. Renew. Sust. Energ. Rev. 161. https://doi.org/10.1016/j.rser.2022.112350.

Hersbach, H., Bell, B., Berrisford, P., Hirahara, S., Horányi, A., Muñoz-Sabater, J., Nicolas, J., Peubey, C., Radu, R., Schepers, D., Simmons, A., Soci, C., Abdalla, S., Abellan, X., Balsamo, G., Bechtold, P., Biavati, G., Bidlot, J., Bonavita, M., De Chiara, G., Dahlgren, P., Dee, D., Diamantakis, M., Dragani, R., Flemming, J., Forbes, R., Fuentes, M., Geer, A., Haimberger, L., Healy, S., Hogan, R.J., Hólm, E., Janisková, M., Keeley, S., Laloyaux, P., Lopez, P., Lupu, C., Radnoti, G., de Rosnay, P., Rozum, I., Vamborg, F., Villaume, S., Thépaut, J.N., 2020. The ERA5 global reanalysis. Q. J. R. Meteorol. Soc. 146, 1999–2049. https://doi.org/10.1002/qj.3803.

Huang, H., Zhu, Z., Li, J., 2024. Disentangling the Unprecedented Yangtze River Basin Extreme High Temperatures in Summer 2022: combined Impacts of the Reintensified La Niña and strong positive NAO. J. Clim. 37, 927–942. https://doi.org/10.1175/jcli-d-23-0466.1.

Jeong, Y., Kim, S.W., Kim, J., Shin, D., Kim, J., Park, J.-H., An, S.-I., 2023. Influence of ENSO on Tropospheric ozone Variability in East Asia. J. Geophys. Res. Atmos. 128. https://doi.org/10.1029/2023JD038604.

Ji, L., Chen, H., 2024. Differences in Variations of Long-Lived and Short-Lived Summer Heat Waves during 1981–2020 over Eastern China and their corresponding Large-Scale Circulation Anomalies. J. Meteorol. Res. 38, 414–436. https://doi.org/10.1007/s13351-024-3162-6.

Jia, X., Chen, X., Dong, W., Ma, H., Ge, J., Qian, Q., 2025. Impact of Tibetan plateau warming amplification on the interannual variations in East Asia Summer precipitation. npj Clim. Atmosphe. Sci. 8. https://doi.org/10.1038/s41612-025-00920-5.

Jiang, Z., Li, J., 2022. Impact of eastern and Central Pacific El Niño on lower tropospheric ozone in China. Atmos. Chem. Phys. 22, 7273–7285. https://doi.org/10.5194/acp-22-7273-2022.

Jiang, L., Peng, H., Zhou, Y., Dai, C., 2025. Current progress on tropospheric ozone sources, biological effects and trends. Int. J. Biometeorol. https://doi.org/10.1007/s00484-025-03010-6.

Kerr, G.H., Waugh, D.W., Steenrod, S.D., Strode, S.A., Strahan, S.E., 2020. Surface Ozone-Meteorology Relationships: Spatial Variations and the Role of the Jet Stream. J. Geophys. Res. Atmos. 125. https://doi.org/10.1029/2020jd032735.

Kong, Q., Guerreiro, S.B., Blenkinsop, S., Li, X.-F., Fowler, H.J., 2020. Increases in summertime concurrent drought and heatwave in Eastern China. Weather and Climate Extremes 28. https://doi.org/10.1016/j.wace.2019.100242.

Kong, X., Kong, L., Chen, D., Liu, S., Feng, M., Tan, Q., Zhou, L., Yang, F., 2025. The Impact of Extreme Summer Heat on VOC Sensitivity and ozone Formation: Insights from Field Campaigns in a Sichuan Basin Megacity, China. J. Geophys. Res. Atmos. 130. https://doi.org/10.1029/2024jd042945.

Kou, W., Gao, Y., Zhang, S., Cai, W., Geng, G., Davis, S.J., Wang, H., Guo, X., Cheng, W., Zeng, X., Ma, M., Wang, H., Wang, Q., Yao, X., Gao, H., Wu, L., 2023. High downward surface solar radiation conducive to ozone pollution more frequent under global warming. Sci. Bull. 68, 388–392. https://doi.org/10.1016/j.scib.2023.01.022.

Krug, A., Fenner, D., Holtmann, A., Scherer, D., 2019. Occurrence and Coupling of Heat and ozone events and their Relation to Mortality rates in Berlin, Germany, between 2000 and 2014. Atmosphere 10. https://doi.org/10.3390/atmos10060348.

Lee, Y.C., Shindell, D.T., Faluvegi, G., Wenig, M., Lam, Y.F., Ning, Z., Hao, S., Lai, C.S., 2014. Increase of ozone concentrations, its temperature sensitivity and the precursor factor in South China. Tellus Ser. B Chem. Phys. Meteorol. 66. https://doi.org/10.3402/tellusb.v66.23455.

Li, Q., Huang, J., 2011. Threshold Values on Extreme High Temperature events in China. J. Appl. Meteorol. Sci. 22, 138–144.

Li, X., Wu, Z., Li, Y., Li, Y., 2016. Potential Influence of Arctic Sea Ice to the Interannual Variations of East Asian Spring Precipitation*. J. Clim. 29, 2797–2813. https://doi.org/10.1175/jcli-d-15-0128.1.

Li, K., Jacob, D.J., Liao, H., Shen, L., Zhang, Q., Bates, K.H., 2019. Anthropogenic drivers of 2013-2017 trends in summer surface ozone in China. Proc. Natl. Acad. Sci. USA 116, 422–427. https://doi.org/10.1073/pnas.1812168116.

Li, K., Jacob, D.J., Shen, L., Lu, X., De Smedt, I., Liao, H., 2020. Increases in surface ozone pollution in China from 2013 to 2019: anthropogenic and meteorological influences. Atmos. Chem. Phys. 20, 11423–11433. https://doi.org/10.5194/acp-20-11423-2020.

Li, M., Yang, Y., Wang, P., Ji, D., and Liao, H.: Impacts of strong El Niño on summertime near-surface ozone over China, Atmospher. Ocean. Sci. Lett., 15, https://doi.org/10.1016/j.aosl.2022.100193, 2022c.

Li, C., Zhu, Q., Jin, X., Cohen, R.C., 2022a. Elucidating Contributions of Anthropogenic Volatile Organic Compounds and Particulate Matter to ozone Trends over China. Environ. Sci. Technol. 56, 12906–12916. https://doi.org/10.1021/acs.est.2c03315.

Li, J., Hao, X., Liao, H., Wang, Y., Cai, W., Li, K., Yue, X., Yang, Y., Chen, H., Mao, Y., Fu, Y., Chen, L., Zhu, J., 2022b. Winter particulate pollution severity in North China driven by atmospheric teleconnections. Nat. Geosci. 15, 349–355. https://doi.org/10.1038/s41561-022-00933-2.

Li, M., Huang, X., Yan, D., Lai, S., Zhang, Z., Zhu, L., Lu, Y., Jiang, X., Wang, N., Wang, T., Song, Y., Ding, A., 2024. Coping with the concurrent heatwaves and ozone extremes in China under a warming climate. Sci. Bull. 69, 2938–2947. https://doi.org/10.1016/j.scib.2024.05.034.

Li, H., Sun, B., Zhang, Z., Wang, H., Zhou, Y., Zeng, J., Zhou, B., 2025. Compound hot drought events in the Mei-yu region: influences from polar and tropical regions. Sci. Bull. 70, 273–282. https://doi.org/10.1016/j.scib.2024.09.043.

Liu, H., Liu, S., Xue, B., Lv, Z., Meng, Z., Yang, X., Xue, T., Yu, Q., He, K., 2018. Ground-level ozone pollution and its health impacts in China. Atmos. Environ. 173, 223–230. https://doi.org/10.1016/j.atmosenv.2017.11.014.

Liu, L., Gong, H., Wang, L., Chen, W., Wu, R., Tao, W., Dong, Z., Liu, B., 2023. Contribution of atmospheric circulations changes to the variations of summertime lower tropospheric ozone over East Asia during recent decades. Atmos. Res. 292, 106852. https://doi.org/10.1016/j.atmosres.2023.106852.

Liu, Z., Zhou, W., Wang, X., 2024. Extreme Meteorological Drought events over China (1951–2022): Migration patterns, diversity of temperature extremes, and decadal variations. Adv. Atmos. Sci. 41, 2313–2336. https://doi.org/10.1007/s00376-024-4004-2.

Lu, X., Hong, J., Zhang, L., Cooper, O.R., Schultz, M.G., Xu, X., Wang, T., Gao, M., Zhao, Y., Zhang, Y., 2018. Severe Surface ozone Pollution in China: a Global Perspective. Environ. Sci. Technol. Lett. 5, 487–494. https://doi.org/10.1021/acs.estlett.8b00366.

Lu, X., Zhang, L., Wang, X., Gao, M., Li, K., Zhang, Y., Yue, X., Zhang, Y., 2020. Rapid increases in Warm-season Surface ozone and Resulting Health Impact in China since 2013. Environ. Sci. Technol. Lett. 7, 240–247. https://doi.org/10.1021/acs.estlett.0c00171.

Luthi, S., Fairless, C., Fischer, E.M., Scovronick, N., Ben, A., Coelho, M., Guo, Y.L., Guo, Y., Honda, Y., Huber, V., Kysely, J., Lavigne, E., Roye, D., Ryti, N., Silva, S., Urban, A., Gasparrini, A., Bresch, D.N., Vicedo-Cabrera, A.M., 2023. Rapid increase in the risk of heat-related mortality. Nat. Commun. 14, 4894. https://doi.org/10.1038/s41467-023-40599-x.

Ma, X., Huang, J., Zhao, T., Liu, C., Zhao, K., Xing, J., Xiao, W., 2021. Rapid increase in summer surface ozone over the North China Plain during 2013–2019: a side effect of particulate matter reduction control? Atmos. Chem. Phys. 21, 1–16. https://doi.org/10.5194/acp-21-1-2021.

Ma, Y.-Y., Chen, Y.-T., Hu, X.-X., Ma, Q.-R., Feng, T.-C., Feng, G.-L., Ma, D., 2023. The 2022 record-breaking high temperature in China: Sub-seasonal stepwise enhanced characteristics, possible causes and its predictability. Adv. Clim. Chang. Res. 14, 651–659. https://doi.org/10.1016/j.accre.2023.09.008.

Martinez-Villalobos, C., Fu, D., Loikith, P.C., Neelin, J.D., 2025. Accelerating increase in the duration of heatwaves under global warming. Nat. Geosci. 18, 716–723. https://doi.org/10.1038/s41561-025-01737-w.

Pu, X., Wang, T.J., Huang, X., Melas, D., Zanis, P., Papanastasiou, D.K., Poupkou, A., 2017. Enhanced surface ozone during the heat wave of 2013 in Yangtze River Delta region. China, Sci. Total Environ. 603-604, 807–816. https://doi.org/10.1016/j.scitotenv.2017.03.056.

Qi, C., Wang, P., Yang, Y., Li, H., Zhang, H., Ren, L., Jin, X., Zhan, C., Tang, J., Liao, H., 2024. Impacts of tropical cyclone–heat wave compound events on surface ozone in eastern China: comparison between the Yangtze River and Pearl River deltas. Atmos. Chem. Phys. 24, 11775–11789. https://doi.org/10.5194/acp-24-11775-2024.

Sun, Y., Chen, H., Zhu, S., Zhang, J., Wei, J., 2021. Influence of the Eurasian Spring Snowmelt on Summer Land Surface Warming over Northeast Asia and its Associated Mechanism. J. Clim. 34, 4851–4869. https://doi.org/10.1175/jcli-d-20-0756.1.

Takaya, K., Nakamura, H., 2001. A Formulation of a Phase-Independent Wave-activity Flux for Stationary and Migratory Quasigeostrophic Eddies on a Zonally varying Basic Flow. J. Atmosphe. Sci. - J ATMOS SCI 58, 608–627. https://doi.org/10.1175/1520-0469(2001)058<0608:AFOAPI>2.0.CO;2.

Tang, S., Qiao, S., Wang, B., Liu, F., Zhu, X., Feng, T., Feng, G., Dong, W., 2025. Recent changes in ENSO'S impacts on the summertime circumglobal teleconnection and mid-latitude extremes. Nat. Commun. 16, 646. https://doi.org/10.1038/s41467-025-55925-8.

Tong, L., Zhang, H., Yu, J., He, M., Xu, N., Zhang, J., Qian, F., Feng, J., Xiao, H., 2017. Characteristics of surface ozone and nitrogen oxides at urban, suburban and rural sites in Ningbo, China. Atmos. Res. 187, 57–68. https://doi.org/10.1016/j.atmosres.2016.12.006.

Wang, P., Yang, Y., Li, H., Chen, L., Dang, R., Xue, D., Li, B., Tang, J., Leung, L.R., Liao, H., 2022. North China Plain as a hot spot of ozone pollution exacerbated by extreme high temperatures. Atmos. Chem. Phys. 22, 4705–4719. https://doi.org/10.5194/acp-22-4705-2022.

Wang, L., Yang, X., Dong, J., Yang, Y., Ma, P., Zhao, W., 2023. Evolution of surface ozone pollution pattern in eastern China and its relationship with different intensity heatwaves. Environ. Pollut. 338, 122725. https://doi.org/10.1016/j.envpol.2023.122725.

Wang, N., Wang, H., Huang, X., Chen, X., Zou, Y., Deng, T., Li, T., Lyu, X., Yang, F., 2024. Extreme weather exacerbates ozone pollution in the Pearl River Delta, China: role of natural processes. Atmos. Chem. Phys. 24, 1559–1570. https://doi.org/10.5194/acp-24-1559-2024.

Wei, J., Li, Z., Li, K., Dickerson, R.R., Pinker, R.T., Wang, J., Liu, X., Sun, L., Xue, W., Cribb, M., 2022. Full-coverage mapping and spatiotemporal variations of ground-level ozone (O3) pollution from 2013 to 2020 across China. Remote Sens. Environ. 270, 112775. https://doi.org/10.1016/j.rse.2021.112775.

Wei, J., Han, W., Wang, W., Zhang, L., Rajagopalan, B., 2023. Intensification of heatwaves in China in recent decades: Roles of climate modes. npj Clim. Atmosphe. Sci. 6. https://doi.org/10.1038/s41612-023-00428-w.

Wen, N., Li, L., 2023. Impact of La Niña on the Following-Summer East Asian Precipitation through Intermediate SST Anomalies. J. Clim. 36, 5743–5755. https://doi.org/10.1175/jcli-d-22-0650.1.

Weng, X., Forster, G.L., Nowack, P., 2022. A machine learning approach to quantify meteorological drivers of ozone pollution in China from 2015 to 2019. Atmos. Chem. Phys. 22, 8385–8402. https://doi.org/10.5194/acp-22-8385-2022.

Wie, J., Moon, B.-K., Yeh, S.-W., Park, R.J., Kim, B.-G., 2021. La Niña-related tropospheric column ozone enhancement over East Asia. Atmos. Environ. 261. https://doi.org/10.1016/j.atmosenv.2021.118575.

Wu, R., Yang, S., Liu, S., Sun, L., Lian, Y., Gao, Z., 2010. Changes in the relationship between Northeast China summer temperature and ENSO. J. Geophys. Res. Atmos. 115. https://doi.org/10.1029/2010jd014422.

Xiao, X., Xu, Y., Zhang, X., Wang, F., Lu, X., Cai, Z., Brasseur, G., Gao, M., 2022. Amplified Upward Trend of the Joint Occurrences of Heat and ozone Extremes in China over 2013-20. Bull. Am. Meteorol. Soc. 1, E1330–E1342. https://doi.org/10.1175/BAMS-D-21-0222.1.

Xu, F., Qu, Y., Bento, V.A., Song, H., Qiu, J., Qi, J., Wan, L., Zhang, R., Miao, L., Zhang, X., Wang, Q., 2024a. Understanding Climate Change Impacts on Drought in China over the 21st Century: A Multi-Model Assessment from CMIP6. npj Clim. Atmosphe. Sci. 7. https://doi.org/10.1038/s41612-024-00578-5.

Xu, R., Sun, H., Zhong, Z., Zheng, Y., Liu, T., Li, Y., Liu, L., Luo, L., Wang, S., Lv, Z., Huang, S., Shi, C., Chen, W., Wei, J., Xia, W., Liu, Y., 2024b. Ozone, Heat Wave, and Cardiovascular Disease Mortality: a Population-based Case-Crossover Study. Environ. Sci. Technol. 58, 171–181. https://doi.org/10.1021/acs.est.3c06889.

Yang, Y., Li, M., Wang, H., Li, H., Wang, P., Li, K., Gao, M., Liao, H., 2022. ENSO modulation of summertime tropospheric ozone over China. Environ. Res. Lett. 17. https://doi.org/10.1088/1748-9326/ac54cd.

Yang, Y., Zhou, Y., Wang, H., Li, M., Li, H., Wang, P., Yue, X., Li, K., Zhu, J., Liao, H., 2024. Meteorological characteristics of extreme ozone pollution events in China and their future predictions. Atmos. Chem. Phys. 24, 1177–1191. https://doi.org/10.5194/acp-24-1177-2024.

Yang, Z., Li, K., Liao, H., Chen, L., 2025a. Analysis of Surface ozone Pollution and its Meteorological Causes in China during the Record Summertime Extreme Heat of 2022. Chin. J. Atmos. Sci. 49, 1–12. https://doi.org/10.3878/j.issn.1006-9895.2302.22211.

Yang, Z., Li, Z., Cheng, F., Lv, Q., Li, K., Zhang, T., Zhou, Y., Zhao, B., Xue, W., Wei, J., 2025b. Two-decade surface ozone (O3) pollution in China: Enhanced fine-scale estimations and environmental health implications. Remote Sens. Environ. 317, 114459. https://doi.org/10.1016/j.rse.2024.114459.

Yin, Z., Wang, H., Li, Y., Ma, X., Zhang, X.J.A.C., 2018. Physics: Arctic sea ice, Eurasia teleconnection pattern and summer surface ozone pollution in North China, pp. 1–17.

Yin, Z., Cao, B., Wang, H., 2019. Dominant patterns of summer ozone pollution in eastern China and associated atmospheric circulations. Atmos. Chem. Phys. 19, 13933–13943. https://doi.org/10.5194/acp-19-13933-2019.

Yuan, X., Chen, X., Ochege, F.U., Hamdi, R., Tabari, H., Li, B., He, B., Zhang, C., De Maeyer, P., Luo, G., 2025. Weakening of global terrestrial carbon sequestration capacity under increasing intensity of warm extremes. Nat. Ecol. & Evolut. 9, 124–133. https://doi.org/10.1038/s41559-024-02576-5.

Zhang, R., Zhang, R., Zuo, Z., 2017. Impact of Eurasian Spring Snow Decrement on East Asian Summer Precipitation. J. Clim. 30, 3421–3437. https://doi.org/10.1175/jcli-d-16-0214.1.

Zhang, X., Zhao, L., Cheng, M., Wu, X., Chen, D., 2020. Urban ozone sink inferred from surface measurements in China. J. Clean. Prod. 253, 119881. https://doi.org/10.1016/j.jclepro.2019.119881.

Zhang, K., Li, J., Guo, Z., Liu, S., Zhu, G., Shang, S., Zhang, J., Ng, M.K., Wu, J., 2025a. Heatwaves on the rise: the Role of El Niño-Southern Oscillation and Local Water-Energy Exchanges in Shaping Global patterns. J. Geophys. Res. Atmos. 130. https://doi.org/10.1029/2024jd042446.

Zhang, T., Wang, X., Song, Y., Chen, H., 2025b. Impact of Spring Snow Cover Anomaly over the Russian Far East on the early Summer Precipitation Variability in Northeast China. J. Geophys. Res. Atmos. 130. https://doi.org/10.1029/2024jd042118.

Zheng, B., Tong, D., Li, M., Liu, F., Hong, C., Geng, G., Li, H., Li, X., Peng, L., Qi, J., Yan, L., Zhang, Y., Zhao, H., Zheng, Y., He, K., Zhang, Q., 2018. Trends in China's anthropogenic emissions since 2010 as the consequence of clean air actions. Atmos. Chem. Phys. 18, 14095–14111. https://doi.org/10.5194/acp-18-14095-2018.

Zhou, J., Zuo, Z., He, Q., 2021. Influence of Eurasian Spring Snowmelt on Surface Air Temperature in late Spring and early Summer. J. Clim. 34, 8191–8204. https://doi.org/10.1175/JCLI-D-21-0111.1.

Zong, L., Yang, Y., Xia, H., Gao, M., Sun, Z., Zheng, Z., Li, X., Ning, G., Li, Y., Lolli, S., 2022. Joint occurrence of heatwaves and ozone pollution and increased health risks in Beijing, China: role of synoptic weather pattern and urbanization. Atmos. Chem. Phys. 22, 6523–6538. https://doi.org/10.5194/acp-22-6523-2022.

Zou, S., Sun, F., De Maeyer, P., Voorde, T.V.D., Duan, W., 2025. Escalating socioeconomic exposure to extreme heat in China: a CMIP6-based analysis of future heatwaves across regions and scenarios. Geogr Sustainability 6. https://doi.org/10.1016/j.geosus.2025.100374.